

# Impact of Parameterized Boundary Layer Structure on Tropical Cyclone Rapid Intensification Forecasts in HWRF

JUN A. ZHANG

*NOAA/Atlantic Oceanographic and Meteorological Laboratory/Hurricane Research Division, and Cooperative Institute for Marine and Atmospheric Studies, University of Miami, Miami, Florida*

ROBERT F. ROGERS

*NOAA/Atlantic Oceanographic and Meteorological Laboratory/Hurricane Research Division, Miami, Florida*

VIJAY TALLAPRAGADA

*NOAA/NWS/NCEP/Environmental Modeling Center, College Park, Maryland*

(Manuscript received 5 April 2016, in final form 27 October 2016)

## ABSTRACT

This study evaluates the impact of the modification of the vertical eddy diffusivity ( $K_m$ ) in the boundary layer parameterization of the Hurricane Weather Research and Forecasting (HWRF) Model on forecasts of tropical cyclone (TC) rapid intensification (RI). Composites of HWRF forecasts of Hurricanes Earl (2010) and Karl (2010) were compared for two versions of the planetary boundary layer (PBL) scheme in HWRF. The results show that using a smaller value of  $K_m$ , in better agreement with observations, improves RI forecasts. The composite-mean, inner-core structures for the two sets of runs at the time of RI onset are compared with observational, theoretical, and modeling studies of RI to determine why the runs with reduced  $K_m$  are more likely to undergo RI. It is found that the forecasts with reduced  $K_m$  at the RI onset have a shallower boundary layer with stronger inflow, more unstable near-surface air outside the eyewall, stronger and deeper updrafts in regions farther inward from the radius of maximum wind (RMW), and stronger boundary layer convergence closer to the storm center, although the mean storm intensity (as measured by the 10-m winds) is similar for the two groups. Finally, it is found that the departure of the maximum tangential wind from the gradient wind at the eyewall, and the inward advection of angular momentum outside the eyewall, is much larger in the forecasts with reduced  $K_m$ . This study emphasizes the important role of the boundary layer structure and dynamics in TC intensity change, supporting recent studies emphasizing boundary layer spinup mechanism, and recommends further improvement to the HWRF PBL physics.


## 1. Introduction

Improving track and intensity forecasts of tropical cyclones (TCs) undergoing rapid intensification (RI) is important because underprediction of RI can lead to a heavy loss of life and tremendous financial loss, especially if a TC undergoes RI prior to making landfall in a densely populated coastal city. The physical processes

involved with RI, and intensification more broadly, involve interactions across multiple spatial and temporal scales (Rogers et al. 2013a; Gall et al. 2013). Accurately representing these scale interactions in numerical models is a challenge, and for this reason forecasting RI remains difficult.

Much research has gone into identifying characteristics of the large-scale environment that are conducive to RI. Using data from the operational Statistical Hurricane Intensity Prediction Scheme (SHIPS) model, Kaplan et al. (2015) showed that TCs that undergo RI are situated in regions with lower vertical environmental wind shear, greater upper-level divergence, higher low- to midlevel environmental moisture, and higher oceanic heat content than those that do not. Their results also

---

 Denotes content that is immediately available upon publication as open access.

---

Corresponding author e-mail: Jun A. Zhang, jun.zhang@noaa.gov

suggest that about 25% of the skill of predicting RI<sup>1</sup> for the Atlantic basin is captured by processes that are controlled by the large-scale environment in the RI index of SHIPS. Thus, it is hypothesized that the remainder of the skill is dependent on inner-core physical processes, although chaotic processes in the inner core, such as deep convection, likely limit the predictability of intensity change.

A variety of observational and modeling studies have identified characteristics of the inner core that make TCs more likely to undergo RI. Observational studies using aircraft data have shown that intensifying TCs have a ringlike vorticity structure, while nonintensifying storms have a monopole-like vorticity structure inside the radius of the maximum wind (RMW) (e.g., Kossin and Eastin 2001; Rogers et al. 2013b). Similar analyses have shown the importance of deep convection within the inner core for storms undergoing RI (Kelley et al. 2004; Reasor et al. 2009; Guimond et al. 2010; Rogers et al. 2013b, 2015). Recent studies using passive microwave satellite data have shown that the majority of TCs that undergo RI have a symmetric eyewall prior to RI onset (Jiang 2012; Kieper and Jiang 2012). When TCs are located in a favorable environment with inner-core structures similar to those mentioned above, they often undergo RI (e.g., Schubert et al. 1999; Kossin and Eastin 2001; Braun et al. 2006; Nolan et al. 2007; Reasor et al. 2009; Rogers 2010). However, TCs that are embedded in less favorable environments (e.g., experiencing moderate vertical shear of  $\sim 10 \text{ m s}^{-1}$ ) do occasionally undergo RI as well (e.g., Molinari and Vollaro 2010; Nguyen and Molinari 2012). Hurricanes Earl (2010) and Edouard (2014), are examples of this (e.g., Stevenson et al. 2014; Montgomery et al. 2014; Rogers et al. 2015, 2016; Suslopatina et al. 2015, Zawislak et al. 2016).

Other studies have emphasized the role of planetary boundary layer (PBL) processes in RI, because these processes regulate the radial and vertical distributions of momentum and enthalpy that are closely tied to storm development and intensification (e.g., Ooyama 1969; Emanuel 1995; Bryan 2012; Cione et al. 2013; Kilroy et al. 2016). This impact is highlighted in previous studies that have demonstrated the sensitivity of simulated TC intensity and structure to the choice of surface layer and boundary layer parameterization schemes (Braun and Tao 2000; Nolan et al. 2009a,b; Smith and Thomsen 2010; Kepert 2012; Green and Zhang 2014; Ming and Zhang 2016). In terms of kinematic processes,

some studies have focused on the inflow of angular momentum surfaces in the frictional boundary layer as being important in vortex spinup (e.g., Smith et al. 2009; Montgomery et al. 2014; Sanger et al. 2014). When the inflow in the boundary layer converges absolute angular momentum at a rate that exceeds its reduction due to frictional torque, the TC spins up.

Another set of studies has stressed convergence in the PBL as a forcing mechanism for the initiation of precipitation (Miyamoto and Takemi 2015), with an emphasis on deep convection (Rogers et al. 2013b, 2015, 2016). These arguments invoke the concept of the efficiency of diabatic heating from deep convection (Schubert and Hack 1982; Shapiro and Willoughby 1982; Hack and Schubert 1986; Nolan et al. 2007), particularly when this convection occurs in a region of high inertial stability inside the RMW (Pendergrass and Willoughby 2009; Vigh and Schubert 2009).<sup>2</sup> In addition to kinematic structures, other research has focused on the role of thermodynamic modification of the PBL in facilitating TC intensity change. Convective downdrafts transport low  $\theta_e$  air to the PBL, reducing the local buoyancy of inflowing air and modifying both the radial and azimuthal distribution of deep convection (Riemer et al. 2010; Molinari et al. 2013; Zhang et al. 2013). Such a flushing of the boundary layer can inhibit convection and TC intensification unless the PBL can recover via surface enthalpy fluxes.

As the above discussion highlights, both the kinematic and thermodynamic structures of the inner core of the TC can play a significant role in determining whether RI occurs. The most challenging aspect of RI forecasts is how to more realistically represent the inner-core processes and structures in TC models that are important for RI, because most of the physics schemes in these models were initially designed for coarse resolution and nonhurricane situations. The representation of vertical eddy diffusivity  $K_m$  in the PBL scheme of the operational Hurricane Weather Research and Forecasting (HWRF) Model was recently upgraded (Tallapragada et al. 2014). These upgrades were based on analyses of in situ aircraft observations of the low-level regions of the hurricane eyewall. (Zhang et al. 2012; Gopalakrishnan et al. 2013). Zhang et al. (2015) found that these upgrades improved the simulated track and intensity of four hurricanes using retrospective HWRF forecasts. They also emphasized the use of *structural*

---

<sup>1</sup> RI, in this context, is defined as an increase in hurricane intensity (measured by the maximum 1-min sustained 10-m wind speed) by a minimum of 30 kt within a 24-h period.

---

<sup>2</sup> Of note, a recent study by Smith and Montgomery (2016) has challenged the applicability of efficiency concepts to interpreting model output or observations. This topic is discussed later in the manuscript.

metrics for model evaluation. These metrics showed substantial improvement in various aspects of the simulated hurricanes, including storm size, surface inflow angle, and kinematic boundary layer height.

While Zhang et al. (2015) documented noteworthy improvements in the TC inner-core structure with improved  $K_m$  based on comparisons of HWRf forecasts with observations at nearly steady-state hurricane stages, no emphasis was placed on examining the aspects of the structure thought to be most important for RI. The present paper aims to further evaluate the impact of  $K_m$  on TC forecasts by focusing on the structures associated with RI. The focus is on identifying the differences in inner-core structures at the onset of RI and relating these differences to the change in the PBL scheme. This task is accomplished by using multiple retrospective HWRf forecasts of TCs that have undergone RI. In addition to documenting the impact of improved  $K_m$  on RI forecasts, such an approach can also aid in identifying the key structures and processes important in predicting RI in HWRf, particularly with respect to the PBL. We note that, while the HWRf PBL scheme still needs further improvements as discussed by Zhang et al. (2015) in the context of the  $K$ -profile parameterizations as detailed by Kepert (2012), we intend to examine differences in the two configurations of  $K_m$  [Eq. (1), see below] in the HWRf PBL scheme to understand why the modified operational scheme is better.

Section 2 gives a brief summary of the model configuration; section 3 presents the impact of the boundary layer physics upgrades on RI forecasts and presents an evaluation of the impact of these upgrades on the simulated structures. Section 4 concludes this paper by discussing possible reasons for these structural differences and their implications for the simulation of RI using HWRf.

## 2. HWRf forecasts and analysis method

The description of the HWRf Model configuration and retrospective forecasts parallel those of Zhang et al. (2015). Below we briefly describe the boundary layer parameterization in the HWRf Model. Details of other aspects of the model setup used to create these forecasts can be found in Zhang et al. (2015).

In the boundary layer scheme, the vertical fluxes of momentum and heat are parameterized using the vertical eddy diffusivity  $K_m$  that has the following form:

$$K_m = \kappa(u^*/\phi_m)z[\alpha(1 - z/h)^2], \quad (1)$$

where  $\kappa = 0.4$  is the Von Kármán constant,  $u^*$  is the surface frictional velocity,  $\phi_m$  is the stability function,  $z$  is

the height,  $h$  is the boundary layer height defined using the bulk Richardson number, and  $\alpha$  is a tuning parameter. During the physics upgrades in 2012,  $\alpha$  was set to 0.5 based on both observational data of Zhang et al. (2011a) and extensive tests based on retrospective runs (Gopalakrishnan et al. 2013; Tallapragada et al. 2014).

A comparison of  $K_m$  in the HWRf Model to observations before and after the physics upgrade is shown in Fig. 1 with Figs. 1c and 1d taken from Zhang et al. (2012) and Zhang et al. (2015). The radius–height plots of  $K_m$  from the two model configurations are also shown in Figs. 1a and 1b. It is evident from Figs. 1c and 1d that the modified  $K_m$  although largely reduced to be much closer to observations at  $\sim 450$ -m altitude, is still larger than the observed values, especially for wind speed  $> 30 \text{ m s}^{-1}$ . The modified  $K_m$  in HWRf has a maximum value of  $50 \text{ m}^2 \text{ s}^{-1}$  at radius of 130 km (Fig. 1f), which is close to the observed maximum value at similar radius given by Zhang and Drennan (2012) based on the in situ data collected during the Coupled Boundary Layers Air–Sea Transfer (CBLAST), while the height of maximum  $K_m$  in HWRf is 150 m higher than that in the observed vertical profile of  $K_m$ . On the other hand, the unmodified  $K_m$  at radius of 130 km in the high- $K_m$  group is significantly larger ( $\sim 3$  times) than the observed values (Fig. 1e) for the entire vertical profile. Of note, in the eyewall region, no observations are available for the vertical profile of  $K_m$ . Although the diagnosed PBL height is significantly reduced (by 2 km) in the modified scheme, it is still much larger ( $\sim 0.5$  km) than the observed value in hurricane conditions as pointed out by Zhang et al. (2015).

As pointed out by Kepert [2012, their Eq. (14), p. 1432], the maximum value of  $K_m$  in this type of  $K$ -profile parameterization (KPP) schemes is proportional to the PBL depth  $h$ . This tuning method used during the HWRf physics upgrade is unphysical as explained below, although it improved the overall presentation of the hurricane boundary layer (Zhang et al. 2015). This method creates an unphysical mismatch between the PBL scheme and surface layer scheme, preventing the consistency of these two schemes that was the main recommendation of Kepert (2012) to the hurricane research community. Note that this underlying problem in the HWRf PBL scheme has been pointed out to the HWRf developers. Further modifications, including replacement of the existing scheme, may produce improved results, but this requires extensive testing. Nonetheless, our paper focuses on demonstrating the sensitivity of RI occurrence to PBL structure (i.e., differences in the depth and strength of the inflow) using the existing HWRf PBL schemes. The tool we are using to demonstrate this impact is the HWRf Model, and the sensitivity was created by this (arbitrary) modification of the  $\alpha$  parameter.

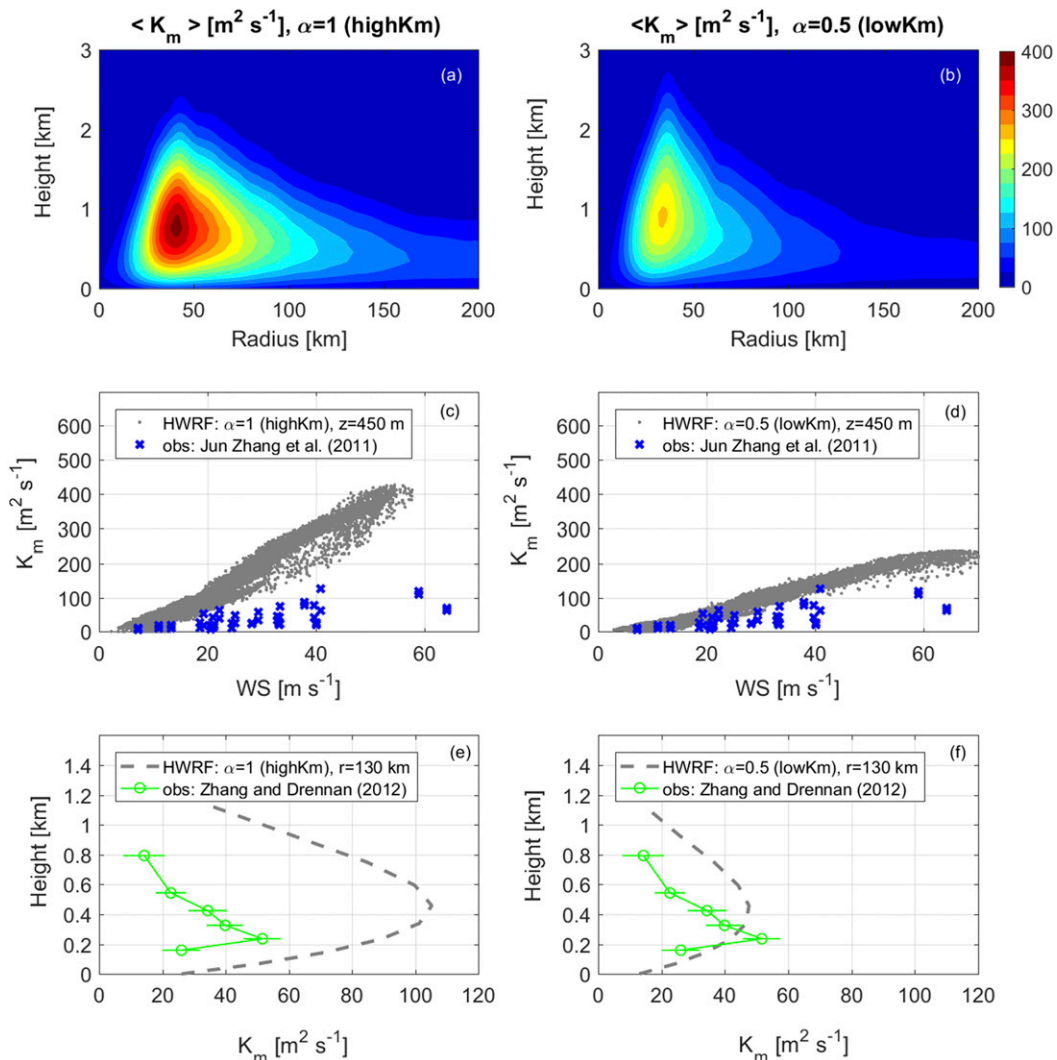


FIG. 1. Comparison of vertical eddy diffusivity ( $K_m$ ) between model simulations and observations. (a),(b) The height–radius plot of azimuthally averaged  $K_m$  ( $\langle K_m \rangle$ ) for the two sets of HWRP forecasts are shown. Boundary layer schemes as in the (a),(c),(e) 2011 ( $\alpha = 1$ , high- $K_m$ ) and (b),(d),(f) 2012 ( $\alpha = 0.5$ , low- $K_m$ ) versions of the HWRP model, respectively. In (c),(d), observations shown by the blue  $\times$ s are from Zhang et al. (2011a), which are based on in situ data at 450-m altitude. In (e),(f), observations shown by the green lines are from Zhang and Drennan (2012), which are based on in situ data at 150-km radius. Panels (c) and (d) are reproduced from Zhang et al. (2012) and Gopalakrishnan et al. (2013).

As stated in Zhang et al. (2015), to evaluate the effect of boundary layer physics upgrade on TC track and intensity forecasts, two sets of retrospective forecasts were run: one with the PBL scheme as in the 2012 operational HWRP Model (hereafter low- $K_m$ ), and the other with the PBL scheme from the 2011 version HWRP (hereafter high- $K_m$ ). These forecasts were performed every 6 h with 3-km horizontal grid resolution for the inner nest in a cycling mode. Each cycle contains a 5-day forecast using the same initial conditions, boundary conditions, and physics packages, except for the parameterization of  $K_m$  as discussed above.

In this study, we used the HWRP forecasts of Hurricanes Earl (2010) and Karl (2010) to evaluate the impact of  $K_m$  on RI forecasts. RI is defined using the threshold of an increase in intensity of  $15 \text{ m s}^{-1}$  ( $\sim 30 \text{ kt}$ ) in 24 h, as in Kaplan et al. (2010). Table 1 summarizes the number of cycles of forecasts and the starting time of the first and last cycles.<sup>3</sup> These forecasts are compared against the best track intensities for Earl and Karl and categorized into four

<sup>3</sup> Table 1 does not include the time periods for when Hurricanes Earl and Karl were either over land and/or were extratropical.

TABLE 1. Summary of storm information and HWRF simulations.

Storm name	No. of cycles of simulations	Starting time of the first cycle	Starting time of the last cycle
Earl	40	1800 UTC 25 Aug 2010	1200 UTC 4 Sep 2010
Karl	15	1800 UTC 14 Sep 2010	0600 UTC 18 Sep 2010

TABLE 2. Contingency table of RI forecasts for low- $K_m$  and high- $K_m$ .

		Observed	
		Yes	No
low- $K_m$	Yes	Hit 16	False Alarm 8
	No	Miss 2	—
high- $K_m$	Yes	Hit 4	False Alarm 0
	No	Miss 14	—

groups: captured RI (“Hit,” defined as when the forecasted RI onset time is within  $\pm 6$  h of the observed RI onset), missed RI (“Miss”), predicted RI with false alarm (“False Alarm”), and correctly rejected RI events based on their RI forecast performance as shown in the contingency table (Table 2). Note that RI onset is defined as the hour in which a single isolated RI event, or the first in a sequence of RI events, occurs. The same metric is used for both of the HWRF forecasts and the best track during verification.

The same structural metrics developed by Zhang et al. (2015) are used in the model diagnostics in a composite framework. In addition to these metrics, we also used other vortex-scale structural metrics from previous observational composite studies on RI processes (e.g., Rogers et al. 2013b), such as inertial stability. A gradient wind strength<sup>4</sup> is another metric evaluated in the present study. As mentioned earlier, our aim is to identify key structural differences at the onset of RI in response to different configurations of  $K_m$ . Thus, we composite modeled fields for 12 h before RI onset ( $t_{RI} - 12$  h) to the time of RI onset ( $t_{RI}$ ) when the low- $K_m$  group forecasted RI and the high- $K_m$  group did not. Composites of the 12-h time period leading up to RI onset from a total of 22 runs were created. We also composite model simulations in the same framework as in our previous observational composite analyses (e.g., Lorsolo et al. 2010; Zhang et al. 2011b; Rogers et al. 2013b), in that the model output was azimuthally averaged as a function of the height and radial distance normalized by the radius of the maximum azimuthally averaged tangential wind speed at 2 km (RMW). Note that the present study focuses on composite analyses of the axisymmetric structure only, while a subsequent paper will evaluate the detailed asymmetric structure and vortex–shear interaction in a case study.

### 3. Results

Table 2 summarizes the number of Hit, Miss, and False Alarm cases. There are many more Hit cases in

low- $K_m$  forecasts than high- $K_m$  forecasts (16 vs 4). The number of Miss cases is substantially smaller in the low- $K_m$  forecasts than in the high- $K_m$  forecasts. There are also more False Alarm cases in low- $K_m$  forecasts than high- $K_m$  forecasts (8 vs 0). Another measure of RI forecast performance is indicated in Fig. 2, which shows a categorical performance diagram (Roebber 2009). This diagram is conceptually similar to the Taylor diagram (Taylor 2001) that measures the forecast performance in terms of probability of detection (POD) and success ratio (SR; the opposite of the false alarm ratio). For good forecasts, both POD and SR approach 1 (i.e., the upper-right corner of the diagram). From Fig. 2, the combined POD and SR score for the low- $K_m$  group is  $\sim 0.61$ , whereas the combined score for the high- $K_m$  group is  $\sim 0.22$ . These results suggest that the low- $K_m$  group performed substantially better for RI forecasts for these cases than the high- $K_m$  group.

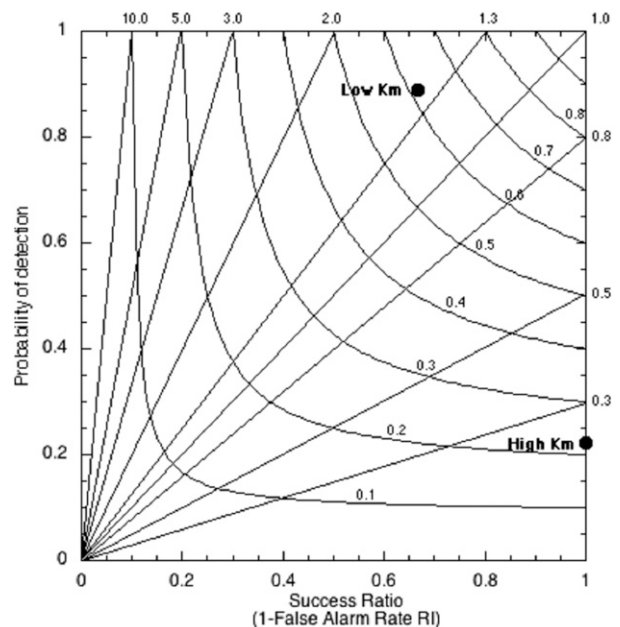


FIG. 2. RI verification using the categorical performance diagram for the low- $K_m$  and high- $K_m$  groups. Note that a perfect forecast lies in the top right of the diagram when the probability of detection (POD) and success ratio (SR) approach unity.

<sup>4</sup> A gradient wind strength is defined as the ratio of a gradient wind speed to the tangential wind speed at the height of  $V_r$ -max. The agradient wind is the departure of tangential wind from the gradient wind speed.



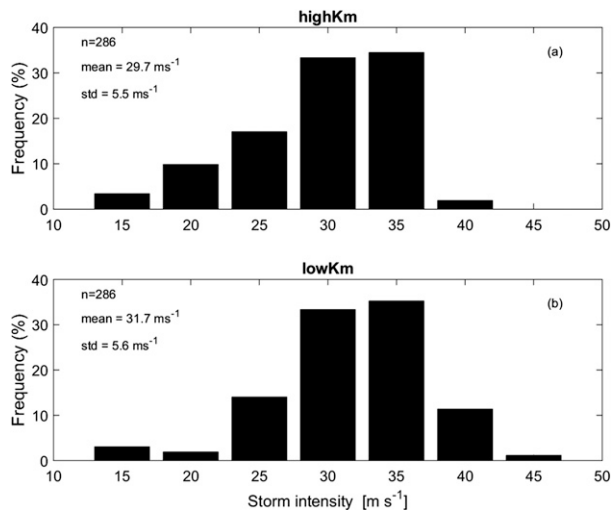


FIG. 3. Frequency distribution of storm intensity ( $\text{m s}^{-1}$ , defined as peak 10-m winds) during the period between 12 h from the onset of RI to the onset of RI for the (a) high- $K_m$  and (b) low- $K_m$  forecasts.

As mentioned earlier, we used the same composite methodology to conduct model diagnostics following our previous study (Zhang et al. 2015). While Zhang et al. (2015) concentrated on evaluating the structures within storms of hurricane strength that ranged from category 1 to category 5 intensity, the forecast samples used in this study focus on the onset of RI, when the storm intensity is close to that of a category 1 hurricane (Fig. 3). Note that the difference in the mean storm intensity (defined as peak 10-m winds) between the low- $K_m$  and high- $K_m$  forecasts is not statistically significant. Figure 4 shows the intensity changes of the RI events, normalized based on the time of RI onset as forecasted in low- $K_m$ , and the corresponding intensity traces from the high- $K_m$  forecasts for those same cycles (Table 2). Only forecasts when low- $K_m$  underwent RI, while high- $K_m$  did not, were used in the composite analyses.<sup>5</sup> It is evident from Fig. 4 that the intensification rate in the 12 h leading up to the onset of RI is essentially the same between the two groups, as indicated by the thick blue and red lines that represent the averaged intensity change for the two groups. After RI onset, however, the intensification rate differs substantially between the two groups of forecasts. In the following composite analysis, we focus on the 12 h leading up to the onset of RI.

A comparison of boundary layer heights is shown in Fig. 5 for high- $K_m$  and low- $K_m$  composites averaged over the 12 h leading up to the RI onset. These heights are defined in several ways, as in Zhang et al. (2011b):

<sup>5</sup> Note that the two RI events correctly forecasted by both low- $K_m$  and high- $K_m$  are not included in the analyses.

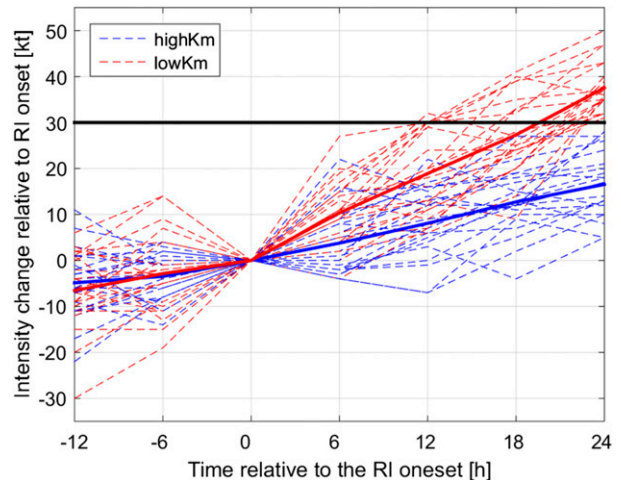


FIG. 4. The 24-h intensity change relative to the onset of RI from the two sets of HWRf forecasts with high- $K_m$  and low- $K_m$  listed in Table 1. The black line shows the RI threshold of 30-kt intensity change in 24 h. The thick blue and red lines are the averages of the dashed blue and red lines, respectively.

the height of the maximum tangential wind speed ( $h_{v_{\text{tmax}}}$ ); the depth of the inflow layer, defined as the height of the 10% peak inflow ( $h_{\text{inflow}}$ ); and the thermodynamic mixed layer depth, defined as the highest altitude where the vertical gradient of  $\theta_v$  equals  $3 \text{ K km}^{-1}$  ( $Z_{\text{ig}}$ ). The boundary layer heights are plotted as a function of radius normalized by RMW at 2-km altitude ( $r^* = r/\text{RMW}$ ) and dimensional height  $z$ . It is evident from Fig. 5 that both  $h_{v_{\text{tmax}}}$  and  $h_{\text{inflow}}$  are higher in the high- $K_m$  composite than the low- $K_m$  composite, consistent with the findings of Zhang et al. (2015). The shallower boundary layer observed in the low- $K_m$  composite is due to the smaller  $K_m$  used and the larger inertial stability at the top of the boundary layer [cf. Fig. 9 as explained by the boundary layer theory of Kepert and Wang (2001)].

It is also evident from Figs. 5c and 5f that the peak tangential and radial velocities are larger in the low- $K_m$  composite than those in the high- $K_m$  composite. In particular, the magnitude of the maximum inflow (minimum  $V_r$ ) is substantially larger in the low- $K_m$  composite than that in the high- $K_m$  composite, and the peak tangential wind at the top of the boundary layer is larger in the low- $K_m$  composite, even though the composite mean intensity, as measured by the peak 10-m wind, is essentially the same for the two composites (cf. Fig. 3). Changing  $K_m$  in the boundary layer led to these structural changes. This result indicates that the azimuthally averaged maximum tangential wind speed may be a better parameter than the 10-m peak wind speed to measure changes in the strength of a TC's primary circulation. A similar approach was followed in recent

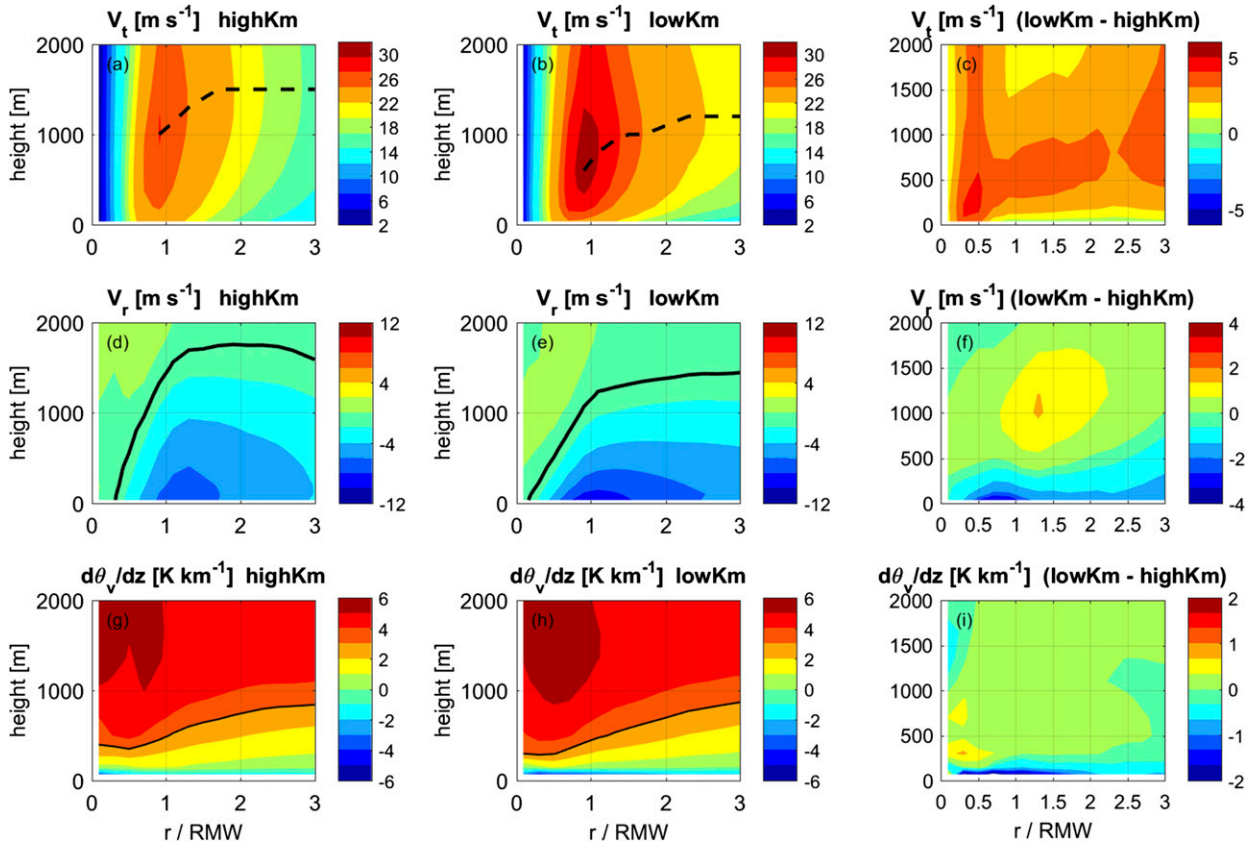


FIG. 5. Azimuthally averaged (a),(b) tangential wind velocity; (d),(e) radial wind velocity; and (g),(h) the vertical gradient of virtual potential temperature as a function of  $r/\text{RMW}$  and height averaged during the period from 12 h before the RI onset to RI onset. (left) High- $K_m$ , (middle) low- $K_m$ , and (right) the difference fields. The dashed lines in (a),(b) represent the height of the maximum tangential wind speed; the solid lines in (d),(e) represent the inflow layer depth defined as the height of the 10% peak inflow. The solid lines in (g),(h) represent the thermodynamic mixed layer depth  $Z_{ig}$ . (c),(f),(i) The difference fields are shown.

studies (e.g., Bryan and Rotunno 2009; Montgomery et al. 2010; Bryan 2012).

Figures 5g and 5h show that the profiles of  $Z_{ig}$  in the high- $K_m$  and low- $K_m$  composites are generally similar, with the low- $K_m$  composite profile being slightly shallower ( $\sim 30$  m) in the eyewall region. Both low- $K_m$  and high- $K_m$  composites show a stable layer above the boundary layer inside the eyewall (Fig. 5i). Kepert et al. (2016) pointed out that this stable layer in the upper part of the inflow layer is largely due to diabatic effects. In the lowest 100 m, the low- $K_m$  composite shows a more unstable layer outside of  $r^* = 1$  than the high- $K_m$  composite (Fig. 5i), consistent with Zhang et al. (2015). This more unstable surface layer likely causes more surface enthalpy fluxes (Fig. 6) in the low- $K_m$  forecasts that are warming and moistening the surface and boundary layer more than in the high- $K_m$  forecasts.

Figure 7 shows that both the boundary layer equivalent potential temperature  $\theta_e$  and relative humidity (RH) are substantially higher in the low- $K_m$  composite than in the high- $K_m$  composite. Overall, the boundary

layer in the low- $K_m$  composite has larger values of  $\theta_e$ , except near the top of the boundary layer at outer radii, which may be due to different boundary layer heights. A similar low-level structure of axisymmetric  $\theta_e$  was shown in Riemer et al. (2010). That study, however, focused on the role of vortex tilt in forcing asymmetries in convection and PBL modification. It is also of note that the peak RH in both composites is  $>90\%$  (Figs. 7d,e), in agreement with the lower bound given by Kieu et al. (2014) for simulating RI storms using HWRF.

Surface inflow angle is an important dynamical parameter for the boundary layer because it is a measure of the relative strength of the secondary and primary circulations (Malkus and Riehl 1960; Kepert 2001; Bryan 2012). A recent observational study by Zhang and Uhlhorn (2012) pointed out that the surface inflow angle is nearly constant with radius outside of the RMW, with a value of  $\sim 22.6^\circ$  for hurricane conditions. They found that there is a weak dependence of the axisymmetric inflow angle on storm intensity. For a category 1 hurricane, the mean inflow angle is  $\sim 20^\circ$ . Figure 8

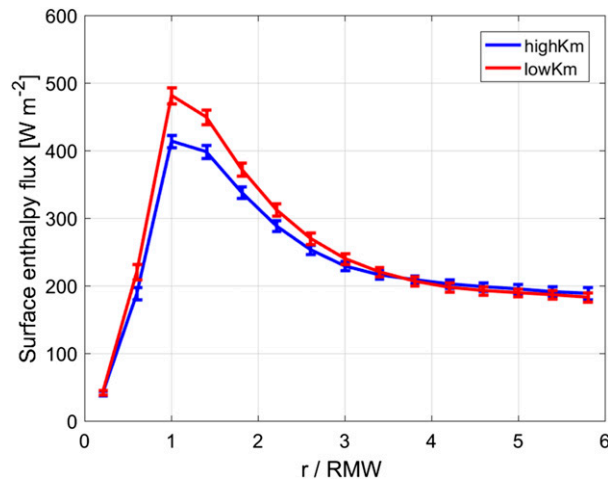


FIG. 6. Surface enthalpy flux as a function of radius to the storm center normalized by the radius of maximum wind speed for the high- $K_m$  and low- $K_m$  composites.

compares the azimuthally averaged surface inflow angle between the high- $K_m$  and low- $K_m$  composites. The surface inflow angle is much larger for low- $K_m$ , consistent with the stronger inflow shown in Figs. 5d and 5e and in better agreement with the observations of Zhang and Uhlhorn (2012).

The azimuthally averaged inertial stability  $I$  and vertical velocity  $w$  are compared in Fig. 9 between the high- $K_m$  and low- $K_m$  composites. The inertial stability of the vortex, especially inside the RMW, is substantially larger in the low- $K_m$  composite than in the high- $K_m$  composite (Figs. 9a–c). Theoretical studies suggest that storms with diabatic heating occurring in an environment of larger inertial stability inside the RMW are more efficient at converting heat release into an increase of the primary circulation (e.g., Nolan et al. 2007; Vigh and Schubert 2009). Figures 9d–f show that the low- $K_m$  composite has a substantially larger azimuthal-mean  $w$  than the high- $K_m$  composite inside the RMW. While this could simply reflect a stronger secondary circulation, consistent with the stronger primary circulation shown in Fig. 5, the difference field for  $w$  (Fig. 9f) shows that the higher value of updrafts for low- $K_m$  is maximized at about  $0.5 \times \text{RMW}$  between 6- and 8-km altitude. The altitude of this peak in the difference field for vertical velocity is above the melting level, suggesting a more prominent role for ice-phase processes and indicating the likely presence of more (and potentially stronger) convection in low- $K_m$  for this radial band. Such an increased coverage of convection in low- $K_m$  may be related to the less stable near-surface layer (cf. Figs. 5g,h). It may also be related to differences in the strength and radial location of boundary layer convergence, since this can play an important role in governing the location of

precipitation and TC intensification (e.g., Miyamoto and Takemi 2015).

Indeed, the peak convergence in the boundary layer is found to be much larger in the low- $K_m$  composite than the high- $K_m$  composite (Fig. 10). The peak convergence for both high- $K_m$  and low- $K_m$  composites is located inside the RMW and is collocated with the  $w$  maximum above the boundary layer, consistent with mass continuity. A more detailed look at the location of the peak convergence in the boundary layer indicates that it is located much closer to the storm center in the low- $K_m$  composite ( $\sim 0.5 \times \text{RMW}$ ) than in the high- $K_m$  composite ( $\sim 0.75 \times \text{RMW}$ ). These results indicate that lower vertical eddy diffusivity leads to storms with stronger boundary layer convergence closer to the center, stronger eyewall updrafts, and faster spinup rates.

Theories for TC spinup were revisited by Smith et al. (2009) and Montgomery and Smith (2014). They summarized two mechanisms for TC spinup that include the following: 1) the conventional paradigm based on the convergence of angular momentum above the boundary layer as first pointed out by Ooyama (1969), and 2) the convergence of angular momentum within the boundary layer similar to that described by Zhang et al. (2001). Both Smith et al. (2009) and Montgomery and Smith (2014) emphasized the role of the boundary layer unbalanced dynamics (mechanism 2) on the spinup of a TC vortex. This unbalanced dynamics is illustrated through the agradient forcing in that the boundary layer flow is supergradient at the location of maximum winds during TC spinup. As mentioned earlier, we introduced the agradient wind strength as a structural metric for model evaluation. Here, the agradient wind is calculated by subtracting the gradient wind<sup>6</sup> speed from the tangential wind speed. Figure 11 compares the agradient wind strength between the high- $K_m$  and low- $K_m$  forecasts for the hourly outputs during the 12-h period before the RI onset. It is evident that the agradient wind strength is substantially larger for low- $K_m$  forecasts than high- $K_m$  forecasts in most cases, indicating that reducing  $K_m$  creates a region whose flow is more supergradient, spinning up the TC vortex much faster in the low- $K_m$  forecasts than the high- $K_m$  forecasts.

Analysis of the horizontal advection of absolute angular momentum  $M$  in the angular momentum budget also indicates that the advection of  $M$  is substantially larger in the boundary layer of the low- $K_m$  composite than the high- $K_m$  composite (Fig. 12). This result is consistent with the boundary layer mechanism advocated by Montgomery and Smith (2014), which may help explain the role of

<sup>6</sup>The gradient wind is calculated by solving the gradient wind balance equation.



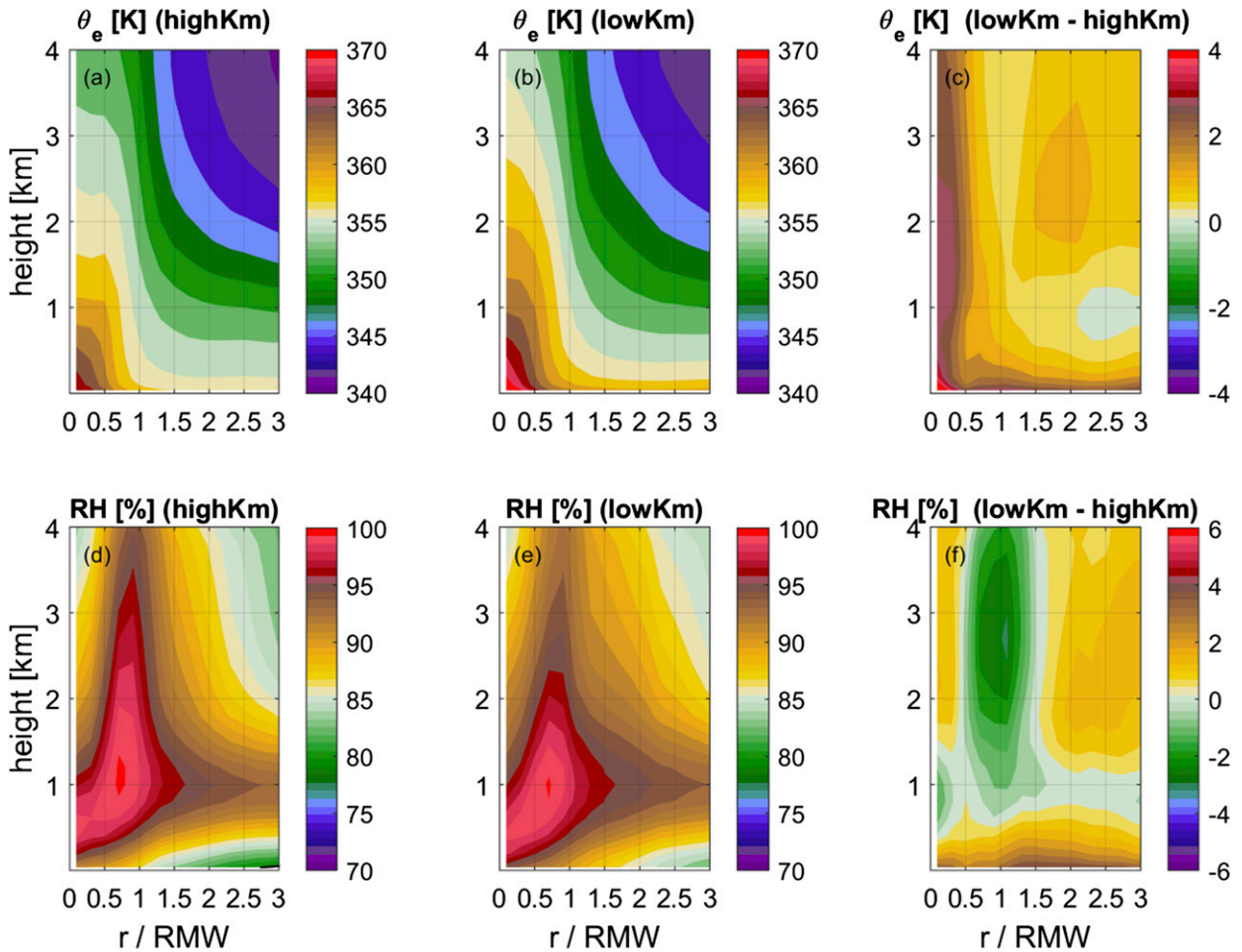


FIG. 7. Azimuthally averaged (a)–(c) equivalent potential temperature  $\theta_e$  and (d)–(f) relative humidity (RH) as a function of  $r/\text{RMW}$  and height. (left) High- $K_m$  and (middle) low- $K_m$ . (right) The difference between the high- $K_m$  and low- $K_m$  composites.

boundary layer vertical eddy diffusivity in governing the simulation of RI storms seen in the HWRf composites. The convergence of angular momentum above the boundary layer (i.e., in the 2–8-km layer) is also larger in the low- $K_m$  composite than in the high- $K_m$  composite (Fig. 12c), consistent with the first mechanism of the TC spinup theory of Smith et al. (2009).<sup>7</sup>

#### 4. Discussion and conclusions

This study evaluates how vertical eddy diffusivity in the boundary layer parameterization scheme in the

operational HWRf Model affects RI forecasts. The results show a significant improvement in the number of RI events with excellent forecasts (Hits), although the number of false alarm forecasts is also larger in response to the improvement of the vertical eddy diffusivity. RI verification using the categorical performance diagram suggests that this improvement in the vertical eddy diffusivity led to improved RI forecasts. Structural metrics are used for model diagnostics in a composite framework. The results show that the simulated TCs with smaller vertical eddy diffusivity (closer to observations) have a shallower boundary layer, stronger inflow in the boundary layer, a more unstable near-surface layer, stronger updrafts within the radius of maximum wind speed, and stronger boundary layer convergence at the onset of RI, although the mean intensity of the storms in the two sets of forecasts is similar.

A comparison of the structures of the high- $K_m$  and low- $K_m$  composites reveals the differences between TCs that rapidly intensify and those that remain steady state

<sup>7</sup> Here, we intend to use the spinup theory to interpret the difference in the RI forecasts of HWRf with two different setups of boundary layer physics using the composite analysis approach. A comprehensive analysis of the angular momentum budget is required to understand the vortex spinup processes related to boundary layer dynamics. This will be done in a case study that is ongoing and will be reported on in a future manuscript.

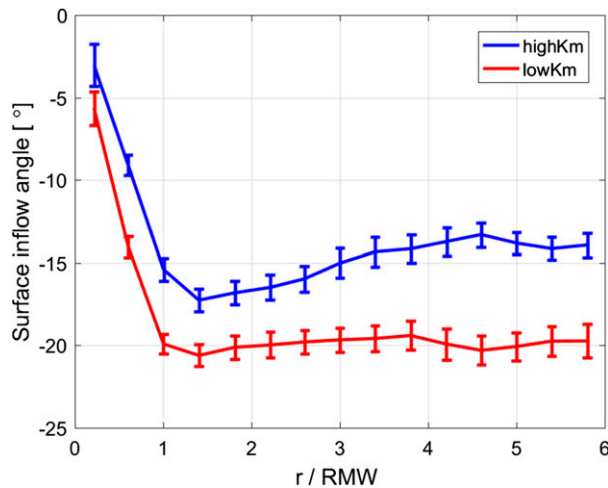


FIG. 8. Surface inflow angle as a function of radius to the storm center normalized by the radius of maximum wind speed for the high- $K_m$  and low- $K_m$  composites.

or slowly intensify in HWRF. Many of the results shown here are quantitatively consistent with those reported by Rogers et al. (2013b), who studied the structural differences between intensifying and steady-state

hurricanes using Doppler radar data. Rogers et al. (2013b) found that storms that intensified faster had stronger updrafts at and inside the RMW, also shown here, and a higher proportion of convective bursts inside the RMW (not shown). However, the inflow layer in the high- $K_m$  composite, which has a slower intensification rate, is deeper, while Rogers et al. (2013b) found that intensifying storms tend to have a deeper inflow layer. This result indicates that the boundary layer height may have less influence on the intensification of a storm than the strength of the inflow. Of note, Doppler radar analyses in Rogers et al. (2013b) do not have data below 500 m. Future work requires analyses of dropsonde data in TCs that under RI to verify the large difference in the strength of the inflow in the boundary layer between the two sets of composites in HWRF.

The preferred location of strong vertical velocity within the high vorticity and inertial stability structure inside the RMW for intensifying storms is consistent with observational (e.g., Rogers et al. 2013b) and theoretical (e.g., Nolan et al. 2007; Vigh and Schubert 2009) studies. The base of the updraft, originating from boundary layer convergence, is located at a smaller

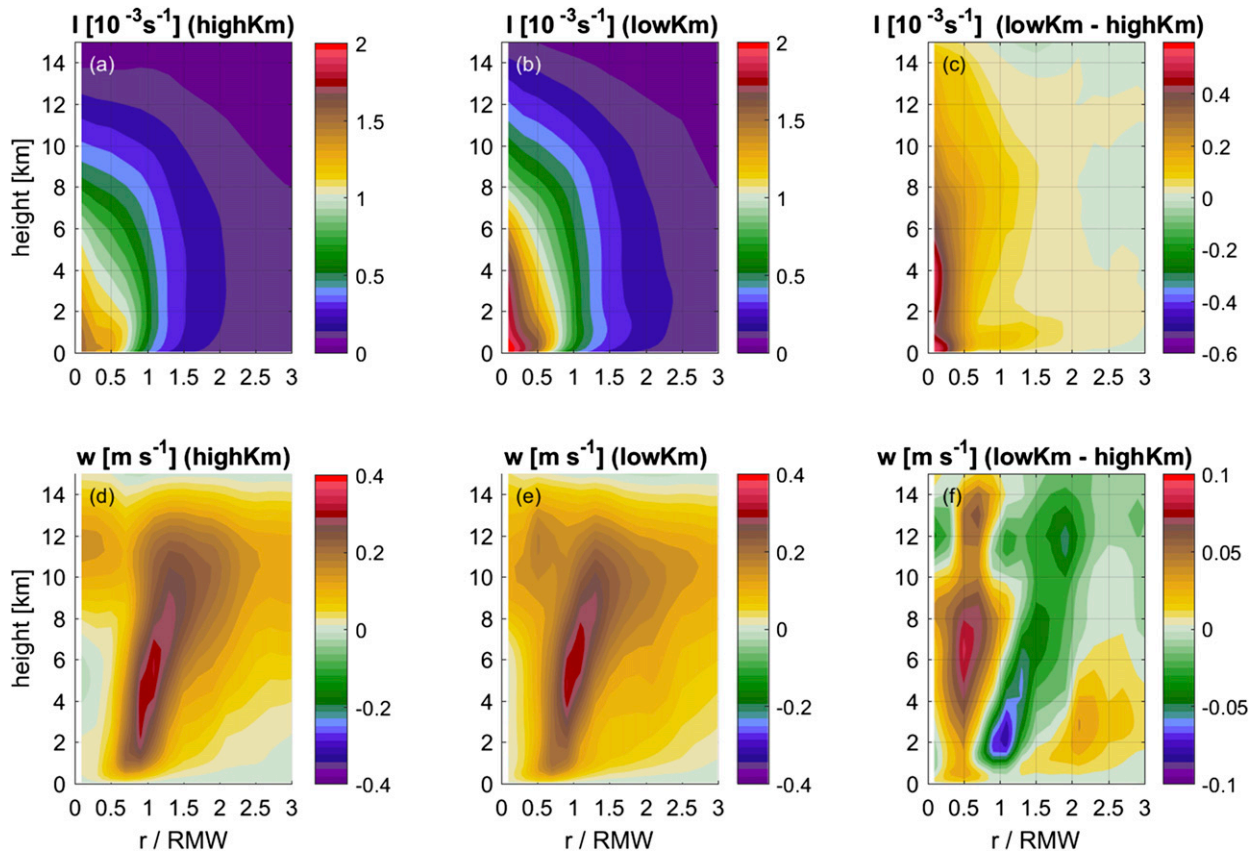


FIG. 9. Azimuthally averaged (top) inertial stability  $I$  and (bottom) vertical velocity  $w$  as a function of  $r/RMW$  and height. (left) High- $K_m$  and (middle) low- $K_m$ . (right) The difference between the high- $K_m$  and low- $K_m$  composites.

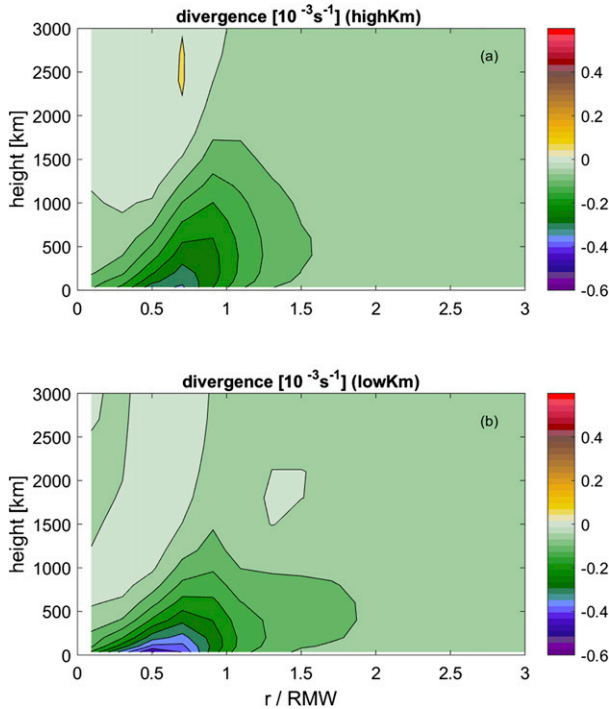


FIG. 10. Azimuthally averaged divergence as a function of  $r/\text{RMW}$  and height for the (a) high- $K_m$  and (b) low- $K_m$  composites.

radius in the low- $K_m$  forecasts, where the inertial stability is higher. In considering the role of deep convection inside the RMW in initiating and promoting RI, Smith and Montgomery (2016) make the point that, rather than making arguments regarding heating efficiency, the role of deep convection can be more succinctly understood simply by considering that angular momentum surfaces are advected inward in the frictional boundary layer when deep convection occurs inside the RMW. Regardless of which role the boundary layer plays in RI (i.e., a direct role involving advection of angular momentum surfaces in the boundary layer versus an indirect role involving forcing of deep convection via boundary layer convergence), both mechanisms require a favorable location of deep convection in a region of enhanced inertial stability (i.e., inside the RMW). The boundary layer vertical eddy diffusivity regulates this boundary layer convergence in HWRf that, in turn, regulates the location of the updrafts.

It is also found that the departure of the maximum tangential wind from the gradient wind balance tends to be larger in the forecasts with reduced vertical eddy diffusivity, which favors a faster spinup of the hurricane vortex. The comparison of gradient wind strength between the two sets of HWRf forecasts is consistent with the spinup theory of Smith et al. (2009). It is the stronger inflow that increases the inward advection of absolute angular

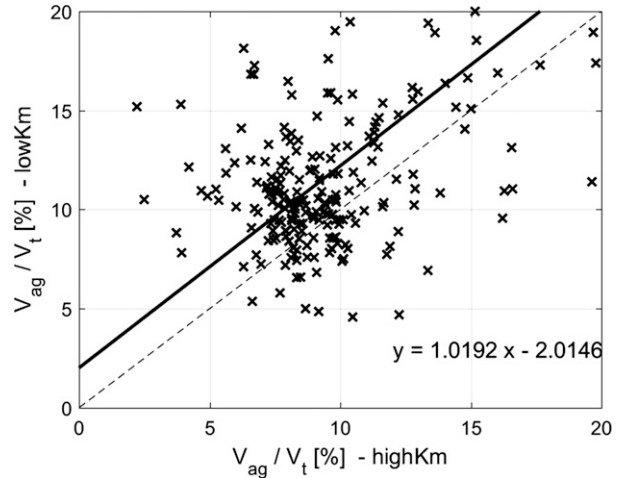


FIG. 11. Comparison of the ratio of gradient and tangential wind speeds at the location of maximum azimuthally averaged tangential wind speed between high- $K_m$  and low- $K_m$  forecasts. The thick black line represents the least squares best fit, and the dashed black line represents the 1:1 ratio.

momentum. The larger tangential wind speeds thereby achieved are associated with a stronger supergradient flow.

Note that Kieu et al. (2014) investigated the vertical structure of TCs at the onset of RI in different environments using idealized HWRf simulations. They found that three conditions had to be reached for the HWRf Model to reproduce RI storms that include 1) a warm core anomaly of 1–3 K, 2) a storm center relative humidity greater than 90%, and 3) a low-level tangential wind speed greater than  $12 \text{ m s}^{-1}$ . The simulated inner-core structures from the HWRf real-case forecasts from our study all reached these three criteria (see Figs. 4, 5, and 7). Nonetheless, our study is the first attempt to evaluate the impact of model physics on RI forecasts in an operational TC model and the TC structure at RI onset.

The results shown here highlight the impact of vertical eddy diffusivity on the structure of TCs that can determine whether RI occurs. A key point of this paper is that it is the whole structure (e.g., tangential wind strength, inflow strength, boundary layer convergence, eyewall updraft strength and depth, inner-core inertial stability), rather than simply the intensity as defined by the peak wind at 10 m, that distinguishes TCs that undergo RI from those that do not. Vertical eddy diffusivity was shown to have a noticeable impact on all of these structural elements in HWRf. The comparison of high- $K_m$  and low- $K_m$  composites shown here documents these differences. A more detailed study investigating the physical processes underlying RI onset in the two formulations of vertical eddy diffusivity is currently being conducted and will be presented in a subsequent paper.

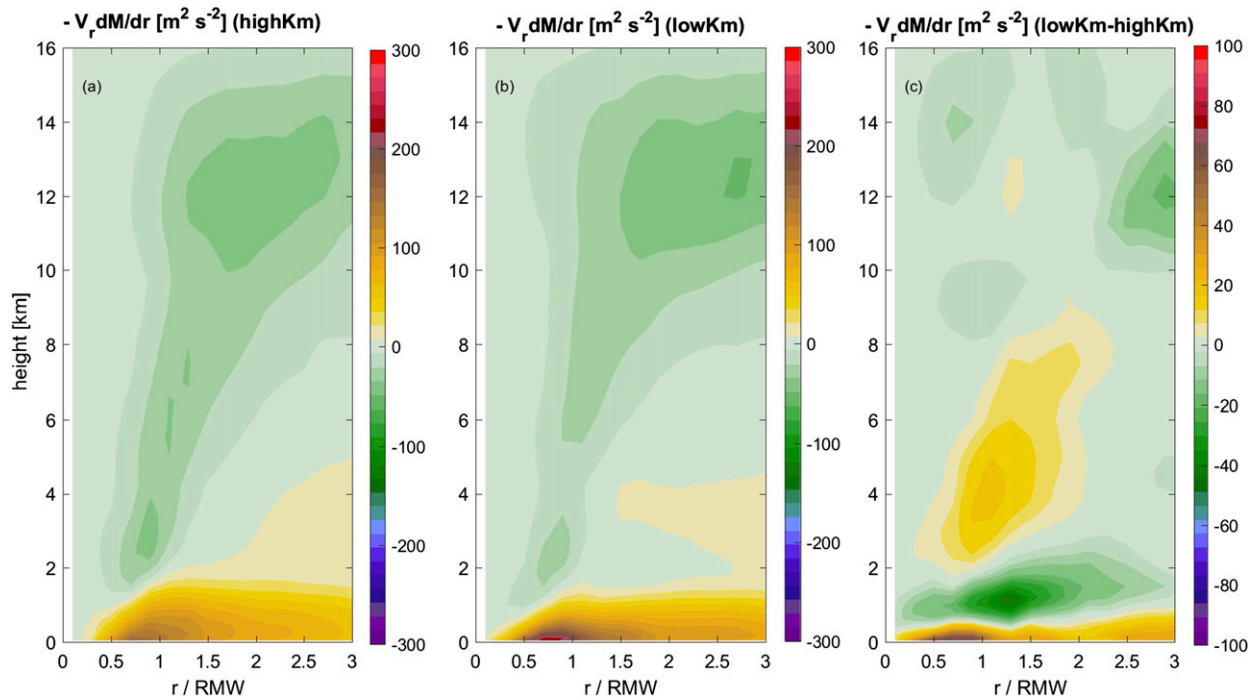


FIG. 12. Azimuthally averaged radial advection of absolute angular momentum ( $-V_r dM/dr$ ) as a function of  $r/RMW$  and height for the (a) high- $K_m$  and (b) low- $K_m$  composites, and (c) the difference in this term for the high- $K_m$  and low- $K_m$  composites.

In conclusion, our study further supports the developmental framework for improving hurricane model physics articulated by Zhang et al. (2012). Although the number of TC forecasts used in this study is limited and HWRP PBL scheme must be improved further in the future, we believe our work provides a useful approach for assessing the impact of future model physics upgrades on RI forecasts. Of note, comparisons in the TC structures between the Hits and False Alarms in the low- $K_m$  group show little difference (not shown), suggesting other parts of the model physics other than the PBL scheme may be also important for RI forecasts in HWRP. Future work will include an assessment of the impact of improving horizontal diffusion (Zhang and Marks 2015) on HWRP RI forecasts. Similar tests can be performed with improvements to the microphysical parameterization, resolution increases, etc. Additional cases will be considered as well.

*Acknowledgments.* This work was mainly supported by funding from NOAA's Hurricane Forecast Improvement Project (HFIP) through Award NA14NWS4680028. Jun Zhang was partially supported by NSF Grant AGS1249732, NOAA Grants NA14NWS4680030, and NA14OAR4830172, and NASA Grant NNX14AM69G. We are grateful to John Kaplan for his comments on an early version of the paper. We are also grateful to Gail

Derr for her editorial support. We thank EMC and HRD HWRP team members for their efforts to continually develop the HWRP Model. In particular, we are grateful to Young Kwon, who substantially contributed to creating the HWRP retrospective forecasts used in this study, as well as Weiguo Wang and Thiago Quirino for their assistance in acquiring the HWRP forecasts. We are very grateful to Sim Aberson for his help with the RI verification using the categorical performance diagram. We are also grateful to Frank Marks and Sundararaman Gopalakrishnan for valuable discussions. We thank Editor Ryan Torn, Roger Smith, and two anonymous reviewers for their comments that helped substantially improve the paper.

#### REFERENCES

- Braun, S. A., and W.-K. Tao, 2000: Sensitivity of high-resolution simulations of Hurricane Bob (1991) to planetary boundary layer parameterizations. *Mon. Wea. Rev.*, **128**, 3941–3961, doi:10.1175/1520-0493(2000)129<3941:SOHRSO>2.0.CO;2.
- , M. T. Montgomery, and Z. Pu, 2006: High-resolution simulation of Hurricane Bonnie (1998). Part I: The organization of eyewall vertical motion. *J. Atmos. Sci.*, **63**, 19–42, doi:10.1175/JAS3598.1.
- Bryan, G. H., 2012: Effects of surface exchange coefficients and turbulence length scales on the intensity and structure of numerically simulated hurricanes. *Mon. Wea. Rev.*, **140**, 1125–1143, doi:10.1175/MWR-D-11-00231.1.



- , and R. Rotunno, 2009: The maximum intensity of tropical cyclones in axisymmetry numerical model simulations. *Mon. Wea. Rev.*, **137**, 1770–1789, doi:10.1175/2008MWR2709.1.
- Cione, J. J., E. A. Kalina, J. A. Zhang, and E. W. Uhlhorn, 2013: Observations of air–sea interaction and intensity change in hurricanes. *Mon. Wea. Rev.*, **141**, 2368–2382, doi:10.1175/MWR-D-12-00070.1.
- Emanuel, K. A., 1995: Sensitivity of tropical cyclones to surface exchange coefficients and a revised steady-state model incorporating eye dynamics. *J. Atmos. Sci.*, **52**, 3969–3976, doi:10.1175/1520-0469(1995)052<3969:SOTCTS>2.0.CO;2.
- Gall, R., J. Franklin, F. Marks, E. N. Rappaport, and F. Toepfer, 2013: The Hurricane Forecast Improvement Project. *Bull. Amer. Meteor. Soc.*, **94**, 329–343, doi:10.1175/BAMS-D-12-00071.1.
- Gopalakrishnan, S. G., F. D. Marks Jr., J. A. Zhang, X. Zhang, J.-W. Bao, and V. Tallapragada, 2013: A study of the impacts of vertical diffusion on the structure and intensity of the tropical cyclones using the high-resolution HWRF system. *J. Atmos. Sci.*, **70**, 524–541, doi:10.1175/JAS-D-11-0340.1.
- Green, B. W., and F. Zhang, 2014: Sensitivity of tropical cyclone simulations to parametric uncertainties in air–sea fluxes and implications for parameter estimation. *Mon. Wea. Rev.*, **142**, 2290–2308, doi:10.1175/MWR-D-13-00208.1.
- Guimond, S. R., G. M. Heymsfield, and F. J. Turk, 2010: Multiscale observations of Hurricane Dennis (2005): The effects of hot towers on rapid intensification. *J. Atmos. Sci.*, **67**, 633–654, doi:10.1175/2009JAS3119.1.
- Hack, J. J., and W. H. Schubert, 1986: Nonlinear response of atmospheric vortices to heating by organized cumulus convection. *J. Atmos. Sci.*, **43**, 1559–1573, doi:10.1175/1520-0469(1986)043<1559:NROAVT>2.0.CO;2.
- Jiang, H., 2012: The relationship between tropical cyclone intensity change and the strength of inner-core convection. *Mon. Wea. Rev.*, **140**, 1164–1176, doi:10.1175/MWR-D-11-00134.1.
- Kaplan, J., M. DeMaria, and J. A. Knaff, 2010: A revised tropical cyclone rapid intensification index for the Atlantic and eastern North Pacific basins. *Wea. Forecasting*, **25**, 220–241, doi:10.1175/2009WAF2222280.1.
- , and Coauthors, 2015: Evaluating environmental impacts on tropical cyclone rapid intensification predictability utilizing statistical models. *Wea. Forecasting*, **30**, 1374–1396, doi:10.1175/WAF-D-15-0032.1.
- Kelley, O. A., J. Stout, and J. B. Halverson, 2004: Tall precipitation cells in tropical cyclone eyewalls are associated with tropical cyclone intensification. *Geophys. Res. Lett.*, **31**, L24112, doi:10.1029/2004GL021616.
- Kepert, J. D., 2001: The dynamics of boundary layer jets within the tropical cyclone core. Part I: Linear theory. *J. Atmos. Sci.*, **58**, 2469–2484, doi:10.1175/1520-0469(2001)058<2469:TDOBLJ>2.0.CO;2.
- , 2012: Choosing a boundary layer parameterization for tropical cyclone modeling. *Mon. Wea. Rev.*, **140**, 1427–1445, doi:10.1175/MWR-D-11-00217.1.
- , and Y. Wang, 2001: The dynamics of boundary layer jets within the tropical cyclone core. Part II: Nonlinear enhancement. *J. Atmos. Sci.*, **58**, 2485–2501, doi:10.1175/1520-0469(2001)058<2485:TDOBLJ>2.0.CO;2.
- , J. Schwendike, and H. Ramsay, 2016: Why is the tropical cyclone boundary layer not “well mixed”? *J. Atmos. Sci.*, **73**, 957–973, doi:10.1175/JAS-D-15-0216.1.
- Kieper, M. E., and H. Jiang, 2012: Predicting tropical cyclone rapid intensification using the 37 GHz ring pattern identified from passive microwave measurements. *Geophys. Res. Lett.*, **39**, L13804, doi:10.1029/2012GL052115.
- Kieu, C., V. Tallapragada, and W. Hogsett, 2014: Vertical structure of tropical cyclones at onset of the rapid intensification in HWRF model. *Geophys. Res. Lett.*, **41**, 3298–3306, doi:10.1002/2014GL059584.
- Kilroy, G., R. K. Smith, and M. T. Montgomery, 2016: Why do model tropical cyclones grow progressively in size and decay in intensity after reaching maturity? *J. Atmos. Sci.*, **73**, 487–503, doi:10.1175/JAS-D-15-0157.1.
- Kossin, J. P., and M. Eastin, 2001: Two distinct regimes in the kinematic and thermodynamic structure of the hurricane eye and eyewall. *J. Atmos. Sci.*, **58**, 1079–1090, doi:10.1175/1520-0469(2001)058<1079:TDRITK>2.0.CO;2.
- Lorsolo, S., J. A. Zhang, F. D. Marks, and J. Gamache, 2010: Estimation and mapping of hurricane turbulent energy using airborne Doppler measurements. *Mon. Wea. Rev.*, **138**, 3656–3670, doi:10.1175/2010MWR3183.1.
- Malkus, J. S., and H. Riehl, 1960: On the dynamics and energy transformations in steady-state hurricanes. *Tellus*, **12A**, 1–20, doi:10.1111/j.2153-3490.1960.tb01279.x.
- Ming, J., and J. A. Zhang, 2016: Effects of surface flux parameterization on the numerically simulated intensity and structure of Typhoon Morakot (2009). *Adv. Atmos. Sci.*, **33**, 58–72, doi:10.1007/s00376-015-4202-z.
- Miyamoto, Y., and T. Takemi, 2015: A triggering mechanism for rapid intensification of tropical cyclones. *J. Atmos. Sci.*, **72**, 2666–2681, doi:10.1175/JAS-D-14-0193.1.
- Molinari, J., and D. Vollaro, 2010: Rapid intensification of a sheared tropical storm. *Mon. Wea. Rev.*, **138**, 3869–3885, doi:10.1175/2010MWR3378.1.
- , J. Frank, and D. Vollaro, 2013: Convective bursts, downdraft cooling, and boundary layer recovery in a sheared tropical storm. *Mon. Wea. Rev.*, **141**, 1048–1060, doi:10.1175/MWR-D-12-00135.1.
- Montgomery, M. T., and R. K. Smith, 2014: Paradigms for tropical cyclone intensification. *Aust. Meteor. Oceanogr. J.*, **64**, 37–66.
- , —, and S. V. Nguyen, 2010: Sensitivity of tropical cyclone models to the surface exchange coefficients. *Quart. J. Roy. Meteor. Soc.*, **136**, 1945–1953, doi:10.1002/qj.702.
- , J. A. Zhang, and R. K. Smith, 2014: An analysis of the observed low-level structure of rapidly intensifying and mature Hurricane Earl (2010). *Quart. J. Roy. Meteor. Soc.*, **140**, 2132–2146, doi:10.1002/qj.2283.
- Nguyen, L. T., and J. Molinari, 2012: Rapid intensification of a sheared, fast-moving hurricane over the Gulf Stream. *Mon. Wea. Rev.*, **140**, 3361–3378, doi:10.1175/MWR-D-11-00293.1.
- Nolan, D. S., Y. Moon, and D. P. Stern, 2007: Tropical cyclone intensification from asymmetric convection: Energetics and efficiency. *J. Atmos. Sci.*, **64**, 3377–3405, doi:10.1175/JAS3988.1.
- , J. A. Zhang, and D. P. Stern, 2009a: Evaluation of planetary boundary layer parameterizations in tropical cyclones by comparison of in situ data and high-resolution simulations of Hurricane Isabel (2003). Part I: Initialization, maximum winds, and outer core boundary layer structure. *Mon. Wea. Rev.*, **137**, 3651–3674, doi:10.1175/2009MWR2785.1.
- , D. P. Stern, and J. A. Zhang, 2009b: Evaluation of planetary boundary layer parameterizations in tropical cyclones by comparison of in situ data and high-resolution simulations of Hurricane Isabel (2003). Part II: Inner core boundary layer and eyewall structure. *Mon. Wea. Rev.*, **137**, 3675–3698, doi:10.1175/2009MWR2786.1.

- Ooyama, K., 1969: Numerical simulation of the life cycle of tropical cyclones. *J. Atmos. Sci.*, **26**, 3–40, doi:10.1175/1520-0469(1969)026<0003:NSOTLC>2.0.CO;2.
- Pendergrass, A. G., and H. E. Willoughby, 2009: Diabatically induced secondary flows in tropical cyclones. Part I: Quasi-steady forcing. *Mon. Wea. Rev.*, **137**, 805–821, doi:10.1175/2008MWR2657.1.
- Reasor, P. D., M. Eastin, and J. F. Gamache, 2009: Rapidly intensifying Hurricane Guillermo (1997). Part I: Low-wavenumber structure and evolution. *Mon. Wea. Rev.*, **137**, 603–631, doi:10.1175/2008MWR2487.1.
- Riemer, M., M. T. Montgomery, and M. E. Nicholls, 2010: A new paradigm for intensity modification of tropical cyclones: Thermodynamic impact of vertical wind shear on the inflow layer. *Atmos. Chem. Phys.*, **10**, 3163–3188, doi:10.5194/acp-10-3163-2010.
- Roebber, P. J., 2009: Visualizing multiple measures of forecast quality. *Wea. Forecasting*, **24**, 601–608, doi:10.1175/2008WAF2222159.1.
- Rogers, R. F., 2010: Convective-scale structure and evolution during a high-resolution simulation of tropical cyclone rapid intensification. *J. Atmos. Sci.*, **67**, 44–70, doi:10.1175/2009JAS3122.1.
- , and Coauthors, 2013a: NOAA's Hurricane Intensity Forecasting Experiment: A progress report. *Bull. Amer. Meteor. Soc.*, **94**, 859–882, doi:10.1175/BAMS-D-12-00089.1.
- , P. Reasor, and S. Lorsolo, 2013b: Airborne Doppler observations of the inner-core structural differences between intensifying and steady-state tropical cyclones. *Mon. Wea. Rev.*, **141**, 2970–2991, doi:10.1175/MWR-D-12-00357.1.
- , P. D. Reasor, and J. A. Zhang, 2015: Multiscale structure and evolution of Hurricane Earl (2010) during rapid intensification. *Mon. Wea. Rev.*, **143**, 536–562, doi:10.1175/MWR-D-14-00175.1.
- , J. Zhang, J. Zawislak, H. Jiang, G. Alvey, E. Zipser, and S. Stevenson, 2016: Observations of the structure and evolution of Hurricane Edouard (2014) during intensity change. Part II: Kinematic structure and the distribution of deep convection. *Mon. Wea. Rev.*, **144**, 3355–3376, doi:10.1175/MWR-D-16-0017.1.
- Sanger, N. T., M. T. Montgomery, R. K. Smith, and M. M. Bell, 2014: An observational study of tropical cyclone spinup in Supertyphoon Jangmi (2008) from 24 to 27 September. *Mon. Wea. Rev.*, **142**, 3–28, doi:10.1175/MWR-D-12-00306.1.
- Schubert, W. H., and J. J. Hack, 1982: Inertial stability and tropical cyclone development. *J. Atmos. Sci.*, **39**, 1687–1697, doi:10.1175/1520-0469(1982)039<1687:ISATCD>2.0.CO;2.
- , M. T. Montgomery, R. K. Taft, T. A. Guinn, S. R. Fulton, J. P. Kossin, and J. P. Edwards, 1999: Polygonal eyewalls, asymmetric eye contraction, and potential vorticity mixing in hurricanes. *J. Atmos. Sci.*, **56**, 1197–1223, doi:10.1175/1520-0469(1999)056<1197:PEAECA>2.0.CO;2.
- Shapiro, L. J., and H. E. Willoughby, 1982: The response of balanced hurricanes to local sources of heat and momentum. *J. Atmos. Sci.*, **39**, 378–394, doi:10.1175/1520-0469(1982)039<0378:TROBHT>2.0.CO;2.
- Smith, R. K., and G. L. Thomsen, 2010: Dependence of tropical-cyclone intensification on the boundary layer representation in a numerical model. *Quart. J. Roy. Meteor. Soc.*, **136**, 1671–1685, doi:10.1002/qj.687.
- , and M. T. Montgomery, 2016: The efficiency of diabatic heating and tropical cyclone intensification. *Quart. J. Roy. Meteor. Soc.*, **142**, 2081–2086, doi:10.1002/qj.2804.
- , —, and S. V. Nguyen, 2009: Tropical cyclone spin-up revisited. *Quart. J. Roy. Meteor. Soc.*, **135**, 1321–1335, doi:10.1002/qj.428.
- Stevenson, S., K. Corbosiero, and J. Molinari, 2014: The convective evolution and rapid intensification of Hurricane Earl (2010). *Mon. Wea. Rev.*, **142**, 4364–4380, doi:10.1175/MWR-D-14-00078.1.
- Susca-Lopata, G., J. Zawislak, E. Zipser, and R. Rogers, 2015: The role of observed environmental conditions and precipitation evolution in the rapid intensification of Hurricane Earl (2010). *Mon. Wea. Rev.*, **143**, 2207–2223, doi:10.1175/MWR-D-14-00283.1.
- Tallapragada, V., C. Kieu, Y. Kwon, S. Trahan, Q. Liu, Z. Zhang, and I. Kwon, 2014: Evaluation of storm structure from the operational HWRF model during 2012 implementation. *Mon. Wea. Rev.*, **142**, 4308–4325, doi:10.1175/MWR-D-13-00010.1.
- Taylor, K. E., 2001: Summarizing multiple aspects of model performance in a single diagram. *J. Geophys. Res.*, **106**, 7183–7192, doi:10.1029/2000JD900719.
- Vigh, J. L., and W. H. Schubert, 2009: Rapid development of the tropical cyclone warm core. *J. Atmos. Sci.*, **66**, 3335–3350, doi:10.1175/2009JAS3092.1.
- Zawislak, J., H. Jiang, G. R. Alvey, E. Zipser, R. Rogers, J. Zhang, and S. Stevenson, 2016: Observations of the structure and evolution of Hurricane Edouard (2014) during intensity change. Part I: Relationship between the thermodynamic structure and precipitation. *Mon. Wea. Rev.*, **144**, 3333–3354, doi:10.1175/MWR-D-16-0018.1.
- Zhang, D.-L., Y. Liu, and M. K. Yau, 2001: A multiscale numerical study of Hurricane Andrew (1992). Part IV: Unbalanced flows. *Mon. Wea. Rev.*, **129**, 92–107, doi:10.1175/1520-0493(2001)129<0092:AMNSOH>2.0.CO;2.
- Zhang, J. A., and W. M. Drennan, 2012: An observational study of vertical eddy diffusivity in the hurricane boundary layer. *J. Atmos. Sci.*, **69**, 3223–3236, doi:10.1175/JAS-D-11-0348.1.
- , and E. W. Uhlhorn, 2012: Hurricane sea surface inflow angle and an observation-based parametric model. *Mon. Wea. Rev.*, **140**, 3587–3605, doi:10.1175/MWR-D-11-00339.1.
- , and F. D. Marks, 2015: Effects of horizontal eddy diffusivity on tropical cyclone intensity change and structure in idealized three-dimensional numerical simulations. *Mon. Wea. Rev.*, **143**, 3981–3995, doi:10.1175/MWR-D-14-00341.1.
- , —, M. T. Montgomery, and S. Lorsolo, 2011a: An estimation of turbulent characteristics in the low-level region of intense Hurricanes Allen (1980) and Hugo (1989). *Mon. Wea. Rev.*, **139**, 1447–1462, doi:10.1175/2010MWR3435.1.
- , R. F. Rogers, D. S. Nolan, and F. D. Marks, 2011b: On the characteristic height scales of the hurricane boundary layer. *Mon. Wea. Rev.*, **139**, 2523–2535, doi:10.1175/MWR-D-10-05017.1.
- , S. G. Gopalakrishnan, F. D. Marks, R. F. Rogers, and V. Tallapragada, 2012: A developmental framework for improving hurricane model physical parameterization using aircraft observations. *Trop. Cyclone Res. Rev.*, **1**, 419–429.
- , R. F. Rogers, P. Reasor, E. Uhlhorn, and F. D. Marks, 2013: Asymmetric hurricane boundary layer structure from dropsonde composites in relation to the environmental vertical wind shear. *Mon. Wea. Rev.*, **141**, 3968–3984, doi:10.1175/MWR-D-12-00335.1.
- , D. S. Nolan, R. F. Rogers, and V. Tallapragada, 2015: Evaluating the impact of improvements in the boundary layer parameterizations on hurricane intensity and structure forecasts in HWRF. *Mon. Wea. Rev.*, **143**, 3136–3154, doi:10.1175/MWR-D-14-00339.1.